Constraining lepton flavor violating Higgs couplings at the HL-LHC in the vector boson fusion channel

Rahool Kumar Barman*
Department of Physics, Oklahoma State University, Stillwater, Oklahoma 74078, USA

P. S. Bhupal Dev†
Department of Physics and McDonnell Center for the Space Sciences, Washington University, St. Louis, Missouri 63130, USA

Anil Thapa‡
Department of Physics, University of Virginia, Charlottesville, Virginia 22904-4714, USA

(Received 7 December 2022; accepted 20 March 2023; published 18 April 2023)

We explore the parameter space of lepton flavor violating (LFV) neutral Higgs Yukawa couplings with the muon and tau leptons that can be probed at the high-luminosity Large Hadron Collider (HL-LHC) via the vector boson fusion (VBF) Higgs production process. Our projected sensitivities for the Standard Model Higgs (h) LFV branching ratio $\mathrm{Br}(h \to \mu\tau)$ in the $pp \to hjj \to (h \to \mu\tau)jj$ channel at the HL-LHC are contrasted with the current and future low-energy constraints from the anomalous magnetic moment and electric dipole moment of the muon, as well as with other LFV observables, such as $\tau \to 3\mu$ and $\tau \to \mu\gamma$. We also study the LFV prospects of a generic beyond the Standard Model neutral Higgs boson (H) with a mass in the range of $m_H \in [20, 800]$ GeV and give the projected model-independent upper limits on the VBF production cross section of Hjj times the branching ratio of $H \to \mu\tau$ at the HL-LHC. We interpret these results in the context of a two-Higgs doublet model as a case study.

DOI: 10.1103/PhysRevD.107.075018

I. INTRODUCTION

The discovery of the Higgs boson of mass 125 GeV at the LHC [1,2] has opened the possibility to gain deeper insight into the mechanism of electroweak symmetry breaking (EWSB) and to search for beyond the Standard Model (BSM) physics phenomena in the Higgs sector. Although the properties of the 125 GeV Higgs boson are thus far consistent with the Standard Model (SM) expectations [3,4], any statistically significant deviations from the SM predictions in future data could point to a new source of EWSB or some BSM physics close to the electroweak scale. Therefore, it is important to search for nonstandard processes involving the Higgs boson.

Within the SM, the Higgs boson couplings to fermions are flavor diagonal: $Y_{ij} = (m_i/v)\delta_{ij}$, where $v = 246$ GeV is the electroweak vacuum expectation value and m_i are the fermion masses. However, these couplings can be quite different in the presence of new physics. In particular, there exist several BSM scenarios which allow for lepton flavor violating (LFV) couplings of the Higgs boson which are absent in the SM; see e.g. Refs. [5–12].

In the case when the 125 GeV Higgs boson is the only source for EWSB and the BSM physics present in the model consists of heavy fields that can be integrated out [13–16], the Yukawa coupling in the mass basis after EWSB can be written as

$$Y_{ij} = \frac{m_i}{v}\delta_{ij} + \frac{v^2}{\sqrt{2}\Lambda^2}\lambda_{ij}, \tag{1}$$

where Λ is the scale of new physics and λ_{ij} are the coefficients associated with the lowest-dimension (dimension-6) effective operators that modify the Yukawa interactions, namely [17]

$$\mathcal{L} \supset -\frac{\lambda_{ij}}{\Lambda^2}(\overline{f_L}^i f_R^j)\phi(\phi^\dagger\phi) + \mathrm{H.c.}, \tag{2}$$

where ϕ is the SM Higgs doublet field and f_L, f_R are the left- and right-handed SM fermions, respectively. Here λ is

*rahool.barman@okstate.edu
†bdev@wustl.edu
‡wtd8kz@virginia.edu

in principle an arbitrary nondiagonal matrix that can significantly modify the Higgs Yukawa interactions for Λ of the order of electroweak scale. It is worth pointing out that to reproduce the hierarchical spectrum of the SM fermion masses, we need to impose either fine-tuning in Eq. (1) or the naturalness condition for the off-diagonal couplings [18]

$$|Y_{ij}Y_{ji}| \lesssim \frac{m_i m_j}{v^2} \quad \text{for } i \neq j. \tag{3}$$

In the case of an additional Higgs boson ϕ_2 taking part in EWSB, the ϕ_2 boson with the same quantum numbers as $\phi:(\mathbf{2}, 1/2)$ under $SU(2)_L \times U(1)_Y$ can contribute to the quark and lepton masses. This allows the Yukawa couplings of the 125 GeV Higgs boson to be misaligned with respect to the SM. In addition, the new scalar if leptophilic can remain sufficiently light and lead to sizable LFV while satisfying the constraints from flavor changing neutral current (FCNC) as well collider bounds. A concrete example is the lepton-specific two Higgs doublet model (2HDM) [19–21].

Without loss of generality and referring to any specific model, we write the effective LFV Yukawa couplings of the (B)SM Higgs boson to the charged leptons as

$$\mathcal{L}_Y \supset -Y_{ij}\overline{\ell}_{Li}e_{Rj}h(H) + \text{H.c.} \tag{4}$$

with Y_{ij} $(i \neq j)$ as free parameters. We set the diagonal couplings Y_{ii} to their respective SM values, i.e. $Y_{ii} = m_i/v$. The new interactions in Eq. (4) can lead to new LFV Higgs decay modes that may be directly observable in current and future collider experiments. The ATLAS and CMS collaborations have performed several searches to study the LFV decays of the SM Higgs boson in the $h \to e\mu$ [22], $e\tau$ [22–26] and $\mu\tau$ [23–28] channels at the LHC; however, any significant excess over SM expectations is yet to be observed. LFV decays of neutral heavy resonances and heavy Higgs bosons at the LHC have also been investigated in Refs. [29–33] and [34,35], respectively. The prospects of probing LFV signals induced by Higgs at the future lepton [36–40] and hadron [41–50] colliders have also been widely explored.

In this work, we focus on the LFV Higgs signal in the $\mu\tau$ channel that can be effectively probed in a model-independent way at the high-luminosity Large Hadron Collider (HL-LHC) using the vector boson fusion (VBF) channel. We first study the projected sensitivity for LFV decays of the SM-like Higgs boson, $h \to \mu\tau$, in the VBF Higgs production channel, $pp \to (h \to \mu\tau)jj$, at the HL-LHC ($\sqrt{s} = 14$ TeV, $\mathcal{L} = 3$ ab^{-1}). We then perform a detailed collider analysis to explore LFV decays of a BSM Higgs boson H in the VBF production channel, $pp \to (H \to \mu\tau)jj$ for several BSM Higgs masses m_H, and derive "model-agnostic" projected upper limits on the production cross section times $\text{Br}(H \to \mu\tau)$ for $m_H \in [20, 800]$ GeV.

Typically, at the hadron colliders, the major impetus has been on gluon gluon fusion (ggF) Higgs production mode, while LFV Higgs decays in the VBF channel have been much less explored. This bias is understandable since the ggF production rates are much larger than VBF in a typical SM Higgs-like scenario with $m_h \sim 125$ GeV.

As expected, the leading sensitivity in searches for LFV decays of h arises from the non-VBF Higgs production category, largely constituted by ggF production. This is also highlighted in the recent searches by CMS [26] and ATLAS [25], where the limits from VBF signal regions alone are weaker by a factor of few than their non-VBF counterparts. However, the VBF production channel becomes extremely relevant in new physics scenarios with extended Higgs sectors like the singlet and 2HDM extensions. The ggF and VBF production rates become comparable for heavier BSM Higgs states H at masses closer to $\mathcal{O}(1)$ TeV [51,52]. In addition, the distinct phenomenological features of the VBF topology offer better control for signal-to-background discrimination than the ggF signal. Overall, the VBF channel can play a complementary role, if not leading, in the search for LFV decays of BSM Higgs extensions and may lead to exciting theoretical implications for new physics, as we show in this work.

It is worth noting that LFV decays of the (B)SM Higgs boson can also be realized in other Higgs production channels, such as Higgstrahlung process $pp \to Zh(H)$. For a SM-like Higgs scenario with $m_h \sim 125$ GeV, the VBF production cross section is 4.4 times larger than the Zh production rate at the $\sqrt{s} = 14$ TeV LHC [51]. The disparity grows wider at higher Higgs masses; for instance, at $m_H \sim 1$ TeV, the VBF to ZH cross-section ratio is ~292 [51]. Because of considerably smaller cross sections, especially at heavier Higgs masses, the sensitivity for LFV decays of BSM Higgs bosons in the Higgstrahlung channel is expected to be subleading than in ggF and VBF modes in a typical 2HDM extension. Therefore, the Zh mode is not considered in the present analysis.

As for the LFV signal itself, ideally, all three LFV decay channels, $h/H \to e\mu, e\tau$ and $\mu\tau$, should be considered in the search for LFV decays of the (B)SM Higgs bosons. However, the partial decay width of an SM Higgs-like boson into the LFV final states is typically proportional to the mass of the heavier lepton, resulting in a usually suppressed signal rate for the $e\mu$ channel than $e\tau$ and $\mu\tau$. Additionally, the rare μ decay processes typically impose stringent upper limits on $Y_{e\mu}$, thus further restricting the search potential in the $e\mu$ channel. The $e\tau$ and $\mu\tau$ decay channels result in roughly similar sensitivity at the LHC [26]; however, the background simulation for the $e\tau$ channel is more challenging due to relatively more significant contamination from the non-prompt-lepton backgrounds. Moreover, we would also like to connect the LFV signal at HL-LHC with the precision low-energy

observable of muon anomalous magnetic moment [53], for which the loop contribution involving a $\mu\tau$ flavor-violating Higgs is typically enhanced by a factor of m_τ/m_μ [12]. In addition, we find that the low-energy constraint from muon electric dipole moment (EDM) on $Y_{\mu\tau}$ is 10 orders of magnitude less stringent than that on $Y_{e\tau}$ from electron EDM [54], thus making the collider study of the $\mu\tau$ channel more relevant. Because of the above reasons, we only focus on LFV decays of the Higgs boson in the $\mu\tau$ channel.

The rest of the paper is organized as follows. In Sec. II we present various low energy LFV constraints on the Yukawa couplings $Y_{\mu\tau}$ and $Y_{\tau\mu}$. Section III discusses the projected sensitivity of the LFV couplings of the SM Higgs boson at the HL-LHC in the VBF channel. Section IV discusses the HL-LHC reach for a generic BSM Higgs LFV decay, as well as a specific example in 2HDM. We conclude in Sec. V.

II. LOW-ENERGY CONSTRAINTS

The LFV couplings in Eq. (4) are subject to various low energy constraints discussed below.

A. Dipole moment

The CP violating and conserving parts of the Yukawa couplings lead to the electric and magnetic dipole moment of the leptons. The flavor violating neutral Higgs contribution to the anomalous magnetic moment $(g-2)_\mu$ at one loop [55] in the limit $m_i < m_H$ is given by

$$\Delta a_\mu \simeq \frac{\Re(Y_{\mu i}Y_{i\mu})}{4\pi^2}\frac{m_\mu m_i}{m_H^2}\left(-\frac{3}{4}+\log\frac{m_H}{m_i}\right). \tag{5}$$

The difference between the experimentally measured value [53,56] and the theoretical one predicted by the SM [57], $\Delta a_\mu = a_\mu^{\rm exp} - a_\mu^{\rm SM} = (251 \pm 59)\times 10^{-11}$, is of 4.2σ discrepancy.[1] In our case, the dominant contribution arises from a τ-Higgs loop and leads to the relation $\Re(Y_{\mu\tau}Y_{\tau\mu}) \simeq (2.37 \pm 0.56)\times 10^{-3}$ in order to accommodate the $(g-2)_\mu$ anomaly at 1σ for $m_H = 125$ GeV.

On the other hand, the EDM of leptons places constraints on the imaginary part of the Yukawa couplings of the Higgs field. These constraints are only significant when there is a chirality flip in the fermion line inside the loop. Neglecting terms suppressed by m_μ/m_τ and m_ℓ/m_H, muon EDM is given by [64]

$$d_\mu \simeq -\frac{\Im(Y_{\mu\tau}Y_{\tau\mu})}{4\pi^2}\frac{em_\tau}{2m_H^2}\left(-\frac{3}{4}+\log\frac{m_H}{m_\tau}\right). \tag{6}$$

The current upper limit from μEDM measurements $d_\mu \le 1.9\times 10^{-19}$ e-cm [65] translates to an upper bound of $\Im(Y_{\mu\tau}Y_{\tau\mu}) < 1.9$ for $m_H = 125$ GeV. The sensitivity reach of the future projection of μEDM is of the order of 10^{-22} e-cm [66–68], corresponding to $\Im(Y_{\mu\tau}Y_{\tau\mu}) < 6\times 10^{-4}$. The current limits on tau EDM [69,70] and future projections [71] are a couple of orders of magnitude weaker than those for muons.

B. $\ell_i \to \ell_j\gamma$

It is important to point out that the off-diagonal Yukawa couplings Y_{ij} suffer strong constraints from radiative decays like $\tau \to \mu\gamma$. The general expression for the rate of $\ell_1 \to \ell_2\gamma$ decay involving the neutral Higgs and a lepton ℓ in the loop reads as [72]

$$\Gamma^{\text{1-loop}}_{\ell_1\to\ell_2\gamma} = \frac{\alpha_{\rm em}}{144(16\pi^2)^2}\frac{m_1^5}{16m_H^4}\Big[(|Y_{2\ell}Y^*_{1\ell}|^2+|Y_{\ell 1}Y^*_{\ell 2}|^2)\mathcal{F}_1^2(t) + \frac{9m_\ell^2}{m_1^2}(|Y^*_{1\ell}Y^*_{\ell 2}|^2+|Y_{2\ell}Y_{\ell 1}|^2)\mathcal{F}_2^2(t)\Big], \tag{7}$$

where $t = m_\ell^2/m_H^2$, and

$$\mathcal{F}_1(t) = \frac{2+3t-6t^2+t^3+6t\log t}{(t-1)^4}, \qquad \mathcal{F}_2(t) = \frac{3-4t+t^2+2\log t}{(t-1)^3}. \tag{8}$$

The second term in Eq. (7) appears from the chirally enhanced radiative diagrams, whereas the first term has no chirality flip in the fermion line inside the loop. The bounds on the Yukawa couplings as a function of the mediator masses can be derived from the current bound on $\mathrm{Br}(\tau\to\mu\gamma) < 4.4\times 10^{-8}$ [73]. The dominant contribution for one loop arises from a chirally enhanced τ-Higgs loop, giving rise to the constraint $\sqrt{|Y_{\mu\tau}|^2+|Y_{\tau\mu}|^2} < 0.17$ for $m_H = 125$ GeV.

In addition to the one loop contribution to the LFV process $\tau\to\mu\gamma$, the two loop Barr-Zee diagrams are also significant, where the dominant contribution arises from top-Higgs and W-Higgs loops [9]. The relevant rate for $\tau\to\mu\gamma$ reads as

$$\Gamma^{\text{2-loop}}_{\tau\to\mu\gamma} = \frac{\alpha m_\tau^5}{64\pi^4}\frac{|Y^*_{\tau\mu}|^2+|Y_{\mu\tau}|^2}{m_H^4}(-0.082Y_t+0.11)^2, \tag{9}$$

where $Y_t = m_{\rm top}/v$ is the top-quark Yukawa coupling for $m_H = 125$ GeV being the SM Higgs mass. In Eq. (9), the two terms with relative minus sign respectively represent

[1] It should be noted here that a recent lattice simulation result from the BMW collaboration [58] is more consistent with the experimental value [53]. Moreover, recent results from other lattice groups seem to be converging towards the BMW result [59,60]. However, these results are in tension with the low-energy $\sigma(e^+e^-\to\text{hadrons})$ data [61–63], and further investigations are ongoing. Until the dust is settled, we choose to use the discrepancy quoted in Ref. [53].

the terms with top quark and W boson contribution. From this equation, we get $\sqrt{|Y_{\mu\tau}|^2+|Y_{\tau\mu}|^2} < 1.97\times10^{-2}$. The full expression can be found in Ref. [9].

C. Trilepton decay

In addition to the radiative decays, the flavor changing Higgs boson allows tree level trilepton decay $l_i \to l_k \bar{l}_j l_l$. In the limit of massless decay products, the partial decay rate reads as [74]

$$\Gamma_{l_i\to l_k\bar{l}_j l_l} = \frac{1}{6144\pi^3}\frac{m_i^5}{4m_H^4}\left(\frac{1}{(1+\delta_{lk})}(|Y_{ik}^* Y_{jl}^*|^2+|Y_{ki}Y_{lj}|^2) + |Y_{ik}^* Y_{lj}|^2+|Y_{ki}Y_{jl}^*|^2\right). \tag{10}$$

Here δ_{lk} is the symmetry factor. Using the total tau decay width $\Gamma_\tau^{\rm tot} = 2.27\times10^{-12}$ GeV and muon Yukawa coupling $Y_{\mu\mu} = m_\mu/v$, we obtain a bound of $\sqrt{|Y_{\mu\tau}|^2+|Y_{\tau\mu}|^2} < 1.35$ for the SM Higgs case from the experimental limit $\mathrm{Br}(\tau\to3\mu) < 2.1\times10^{-8}$ [75]. It is clear that these tree level decays are suppressed by the muon Yukawa coupling. On the other hand, loop level contributions do not have such suppression and can be dominant. The one loop contribution for $\tau\to3\mu$ is obtained by attaching a muon line to the photon in the radiative decay of $\tau\to\mu\gamma$, which corresponds to a bound of $\sqrt{|Y_{\mu\tau}|^2+|Y_{\tau\mu}|^2} < 0.13$ [9,76]. This however turns out to be weaker than the $\tau\to\mu\gamma$ constraint, as expected.

D. Z-boson decay

In the presence of the Yukawa couplings $Y_{\tau\mu}$ and $Y_{\mu\tau}$, the effective $\mu-\tau-Z$ vertices are induced at one loop order [77]:

$$\Gamma_{Z\to\tau\mu} = \frac{m_Z}{6\pi}\left(\frac{1}{2}|C_L^Z(m_Z^2)|^2+\frac{m_Z^2}{m_\tau^2}|D_L^Z(m_Z^2)|^2+(L\leftrightarrow R)\right), \tag{11}$$

where the coefficients read as

$$C_L^Z(s) = \frac{gY_{\tau\tau}Y_{\tau\mu}}{64\pi^2}(F_V^v(s)g_V^e+F_V^a(s)g_A^e),$$
$$D_L^Z(s) = \frac{gY_{\tau\tau}Y_{\mu\tau}^*}{64\pi^2}(F_D^v(s)g_V^e+F_D^a(s)g_A^e). \tag{12}$$

C_R^Z and D_R^Z are obtained by interchanging $Y_{\tau\mu}\leftrightarrow Y_{\mu\tau}^*$ and $F_{V,D}^a\to-F_{V,D}^a$. The functions $F_{V,D}^{v,a}$ are expressed in terms of Passarino-Veltman functions (see Ref. [77] for details). Numerically the functions $\{F_V^a, F_V^v, F_D^a, F_D^v\}$ at $s=m_Z^2$ read as $\{5-0.78i, -4.8-0.78i, (-8.1+1.6i)\times10^{-5}, 0.84\}$. Using these values and current experimental bound $\mathrm{Br}(Z\to\mu\tau) < 9.5\times10^{-6}$ [78] leads to the relation $\mathrm{Br}(Z\to\mu^\mp\tau^\pm) = 8.9\times10^{-10}|Y_{\mu\tau}|^2+7.7\times10^{-10}|Y_{\tau\mu}|^2$ [76,77]. The upcoming e^+e^- collider such as the FCC-ee has the sensitivity that can prove the LFV decay of Z in $\mu\tau$ decay up to $\mathcal{O}(10^{-9})$ [79].

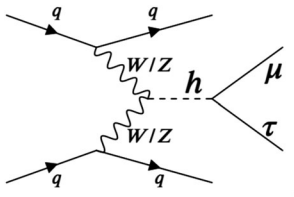

FIG. 1. Leading order Feynman diagram for Higgs production in association with two jets in the vector boson fusion mode.

III. PROJECTED SENSITIVITY AT THE HL-LHC

We study the projected sensitivity for the LFV couplings of the 125 GeV SM Higgs boson at the high luminosity LHC ($\sqrt{s}=14$ TeV, $\mathrm{L}=3\,\mathrm{ab}^{-1}$) through searches in VBF Higgs production channel

$$pp\to hjj\to(h\to\mu\tau)jj, \tag{13}$$

where τ leptons can decay leptonically $\tau_e\to e+\nu_e+\nu_\tau$[2] or hadronically $\tau_h\to$ hadrons $+\,\nu_\tau$. Representative Feynman diagram for the signal is shown in Fig. 1.

Both leptonic and hadronic decay modes of the τ leptons are considered in the present analysis. In the $\mu\tau_e$ channel, we require exactly one isolated muon and one oppositely charged isolated electron in the final state, with $p_{T,\mu/e} > 15$ GeV and $|\eta| < 4.0$. Likewise in the $\mu\tau_h$ channel, we require exactly one isolated muon with the aforesaid trigger cuts and one oppositely charged τ tagged jet with $p_{T,\tau_h} > 25$ GeV and $|\eta| < 4.5$. Both channels are also required to have at least two light flavored jets (j) with $p_T > 30$ GeV and $|\eta| < 4.5$. The η cuts are less stringent than the recent ATLAS [25] and CMS [26] studies in the same channel due to larger η coverage at the HL-LHC [80].

The important backgrounds are $Z+$ jets, $t\bar{t}$, multijet and $W+$ jets with jets misidentified as leptons or τ-tagged jets, and $VV+$ jets, while subleading contributions can arise from single Higgs production in the VBF and gluon-gluon-fusion (ggF) channel with $h\to\tau\tau$ and $h\to W^+W^-$. Furthermore, ggF mediated single Higgs production with LFV Higgs decay can also contribute to the VBF signal [25,81,82]. We generate the signal and background events with `MG5_aMC@NLO` [83–85] at the leading order with $\sqrt{s}=14$ TeV. Signal and background events are simulated with generator-level cuts on the transverse momentum p_T and pseudorapidity η for the light flavored jets and leptons,

[2]Since we have a muon final state from $h\to\mu\tau$, we do not consider the tau decay into muon.

$p_{T,j/\ell} > 10$ GeV and $|\eta_{j\ell}| < 5.0$. A minimum threshold on the dijet invariant mass, $m_{jj} > 300$ GeV, is applied at the generator level for the background events. PYTHIA8 [86] is used for parton showering and hadronization. The detector response is simulated using DELPHES-3.5.0 [87] with the default HL-LHC detector card [88,89].

We closely follow the analysis strategy in a recent ATLAS study for the $\sqrt{s} = 13$ TeV LHC [25]. In the $\mu\tau_e$ channel, the leading and subleading p_T leptons, ℓ_1 and ℓ_2, respectively, are required to satisfy $p_{T,\ell_1} > 45$ GeV and $p_{T,\ell_2} > 15$ GeV. The asymmetric p_T cuts are used to suppress the $h \to \tau^+\tau^-$ background. We also veto events containing a third isolated electron or muon to reduce the diboson background. Similarly, in the $\mu\tau_h$ channel, we require $p_{T,\mu} > 30$ GeV and $p_{T,\tau_h} > 45$ GeV. We also require the sum of cosine of azimuthal angle differences among the $\{\mu, \not{E}_T\}$ and $\{\tau_h, \not{E}_T\}$ pairs, $\sum_{i=\mu,\tau_h} \cos\Delta\Phi(i, \not{E}_T)$, to be greater than > -0.35 in order to reduce the $W+$jets background. Furthermore, an upper limit is imposed on the pseudorapidity difference between μ and τ_h, $|\Delta\eta(\mu, \tau_h)| < 2.0$ to suppress the contributions arising from multijet backgrounds [25]. To reduce the massive $t\bar{t}$ background, events containing any b tagged jet with $p_T > 25$ GeV and $|\eta| < 4.0$ are vetoed in both channels.

The next objective is to identify and reconstruct the VBF topology. The leading and subleading p_T light jets j_1 and j_2, respectively, are tagged as VBF jets provided they satisfy $p_{T,j_1(j_2)} > 40$ GeV (30 GeV). The VBF jets feature a large invariant mass $m_{j_1 j_2}$. Correspondingly, we impose a minimum threshold of $m_{j_1 j_2} > 350$ GeV. Furthermore, the VBF jets are mostly produced back to back in the forward regions of the detector, thus having $\eta_{j_1} \cdot \eta_{j_2} < 0$, and are characterized by a large pseudorapidity difference $|\Delta\eta(j_1, j_2)|$. For illustrative purposes, we present the distributions for $|\Delta\eta(j_1, j_2)|$ in Fig. 2. Since the VBF jets are mostly populated at large $|\Delta\eta(j_1, j_2)|$ regions, we require the events to satisfy $|\Delta\eta(j_1, j_2)| > 2$ at the event selection stage and also use $|\Delta\eta(j_1, j_2)|$ as a training observable in the multivariate analysis. The VBF topology also features reduced jet activity in the central region. Therefore, events with additional light jets (j_3) in the central region are vetoed by imposing $|\eta_{j_3} - (\eta_{j_1} + \eta_{j_2})/2| > 1.0$. The event selection cuts for $\mu\tau_e$ and $\mu\tau_h$ channels are summarized in Table I.

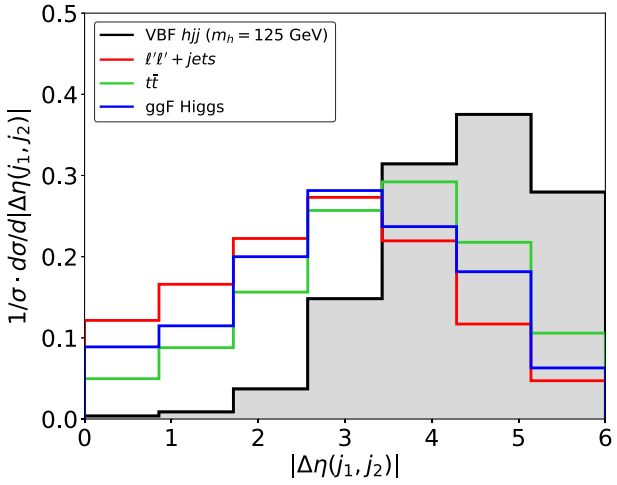

FIG. 2. Distributions for the difference of pseudorapidities for the VBF tagged jets $|\Delta\eta(j_1, j_2)|$ at the detector level for the $\ell'\ell' +$ jets (red) and $t\bar{t}$ (green) backgrounds, $gg \to h_{125}$ (blue) and VBF (black) signal events at $m_h = 125$ GeV. The events satisfy the basic selection cuts for $\mu\tau_e$ channel in Table I, $p_{T,j_1} > 40$ GeV, $p_{T,j_2} > 30$ GeV and $m_{j_1 j_2} > 350$ GeV. We assume $\sqrt{s} = 14$ TeV LHC with $\mathcal{L} = 3$ ab^{-1}.

TABLE I. Summary of event selection cuts for $\mu\tau_e$ and $\mu\tau_h$ channels.

	$\mu\tau_e$	$\mu\tau_h$
Basic selection	$n_\mu = 1$, $n_e = 1$	$n_\mu = 1$, $n_{\tau_h} = 1$
	$(e^+\mu^-/e^-\mu^+)$	$(\tau_h^+\mu^-/\tau_h^-\mu^+)$
	$p_{T,\ell_1} > 45$ GeV	$p_{T,\tau_h} > 45$ GeV
	$p_{T,\ell_2} > 15$ GeV	$p_{T,\mu} > 30$ GeV
	…	$\sum_{i=\mu,\tau_h} \cos\Delta\Phi(i, \not{E}_T) > -0.35$
	…	$\lvert\Delta\eta(\mu, \tau_h)\rvert < 2.0$
	b jet veto if $p_T > 25$ GeV and $\lvert\eta\rvert < 4.0$	
VBF topology	$p_{T,j_1} > 40$ GeV, $p_{T,j_2} > 30$ GeV, $\lvert\Delta\eta(j_1, j_2)\rvert > 2$, $\eta_{j_1} \cdot \eta_{j_2} < 0$, $m_{j_1 j_2} > 350$ GeV $\lvert\eta_{j_3} - (\eta_{j_1} + \eta_{j_2})/2\rvert > 1.0$	

We perform a multivariate analysis using the Boosted Decision Trees (BDT) algorithm to discriminate the VBF signal from SM backgrounds. The kinematic observables used to perform the multivariate analysis are shown in Table II.

Here, $m_T(\alpha, \not{E}_T)(\alpha = \mu, e)$ is the transverse mass for the lepton α and $\not{E}_T$ pair, defined as $m_T(\alpha, \not{E}_T) = \sqrt{2 p_{T,\alpha} \not{E}_T (1 - \cos\Delta\phi(\alpha, \not{E}_T))}$, $\Delta\phi(\beta, \not{E}_T)$ $(\beta = \alpha, \tau_h)$ is the difference in azimuthal angles for object β and $\not{E}_T$, and $m_{\rm vis}$ is the visible invariant mass for the $h \to \mu(\tau \to e\nu_\tau\nu_e)$ system. The full reconstruction of the Higgs boson is challenging since the τ decay is associated with missing energy. Several techniques have been developed to

TABLE II. Input observables used in the BDT analysis for $\mu\tau_e$ and $\mu\tau_h$ channels.

$\mu\tau_e$	$\mu\tau_h$
$p_{T,e}, m_T(e, \not{E}_T)$	$p_{T,\tau_h}, m_T(\tau_h, \not{E}_T)$,
$\Delta R(\mu, e), \Delta\phi(e, \not{E}_T)$	$\Delta R(\mu, \tau_h), \Delta\phi(\tau_h, \not{E}_T)$
$p_{T,e}/p_{T,\mu}, \eta_e, \phi_e$	$\eta_{\tau_h}, \phi_{\tau_h}, \sum_{i=\mu,\tau_h} \cos\Delta\Phi(i, \not{E}_T)$,
$p_{T,\mu}, m_T(\mu, \not{E}_T), \Delta\phi(\mu, \not{E}_T), \eta_\mu, \phi_\mu, \phi_{\not{E}_T}$,	
$m_{\rm coll}, m_{\rm vis}, m_{j_1 j_2}, \Delta\eta(j_1, j_2), \not{E}_T$	

reconstruct the resonant invariant mass in such cases (cf. Refs. [90–92] and references therein). In this analysis, we adopt the collinear mass approximation technique which is rooted on two important assumptions that the visible and invisible decay products of τ are collinear, and the only source of missing energy in the system is the neutrinos from τ decay. Following Ref. [91], the collinear mass is computed as $m_{\rm coll} = m_{\rm vis}/\sqrt{x_{\tau_e}}$, where $x_{\tau_e} = p_{T,\tau_e}/(p_{T,\tau_e} + \not{E}_T)$. The rest of the observables in Table II have their usual meaning.

In Figs. 3 and 4, we show the correlation among the input variables for signal and background events in the $\mu\tau_e$ and $\mu\tau_h$ channels, respectively. Because of high correlation ($\gtrsim$80%) between $m_{\rm coll}$ and $m_{\rm vis}$, the latter is not considered in the training. Similarly, in the $\mu\tau_h$ channel, the highly correlated observable pairs are $\{m_{\rm vis}, m_{\rm coll}\}$ and $\{\Delta\phi(\tau_h, \not{E}_T), m_T(\tau_h, \not{E}_T)\}$, among which, we include only the latter two observables in the training. The kinematic observables from Table II with the highest ranks in the BDT analysis are

$$\mu\tau_e : m_{\rm coll}, m_T(\mu/e, \not{E}_T), \Delta R(\mu, e), \not{E}_T, \Delta\Phi(\mu, \not{E}_T)$$
$$\mu\tau_h : m_{\rm coll}, m_T(\tau_h, \not{E}_T), \Delta\Phi(\mu, \not{E}_T), \Delta\Phi(\mu, \not{E}_T), \not{E}_T, \phi_\mu.$$

In the $\mu\tau_e$ channel, the contribution from multijet events to the total background is expected to be suppressed since the probability for two jets being misidentified as isolated leptons with different flavors is relatively small. Previous searches performed in the aforesaid channel using the LHC run-II data collected at $\mathcal{L} = 36.1$ fb^{-1} [25] indicate that the relative contribution from misidentified backgrounds, which include W + jets and multijet processes, is around 5% of the total background. Therefore, we ignore the misidentified backgrounds in our analysis for the $\mu\tau_e$ channel. However, in the $\mu\tau_h$ channel, misidentified events have a nontrivial contribution. The analysis for the VBF $\mu\tau_h$ channel in Ref. [25] indicates the contribution from misidentified backgrounds to be roughly 25%, and hence, cannot be neglected. However, simulating the QCD multijet and

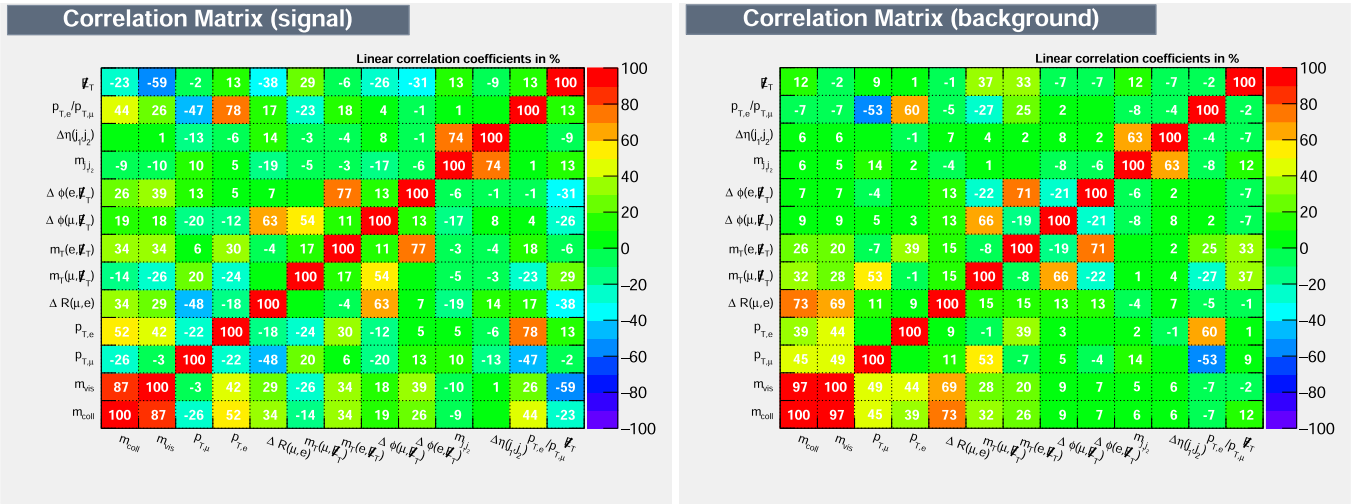

FIG. 3. Linear correlation coefficient matrix for input variables to the BDT for signal and background events in the $\mu\tau_e$ channel.

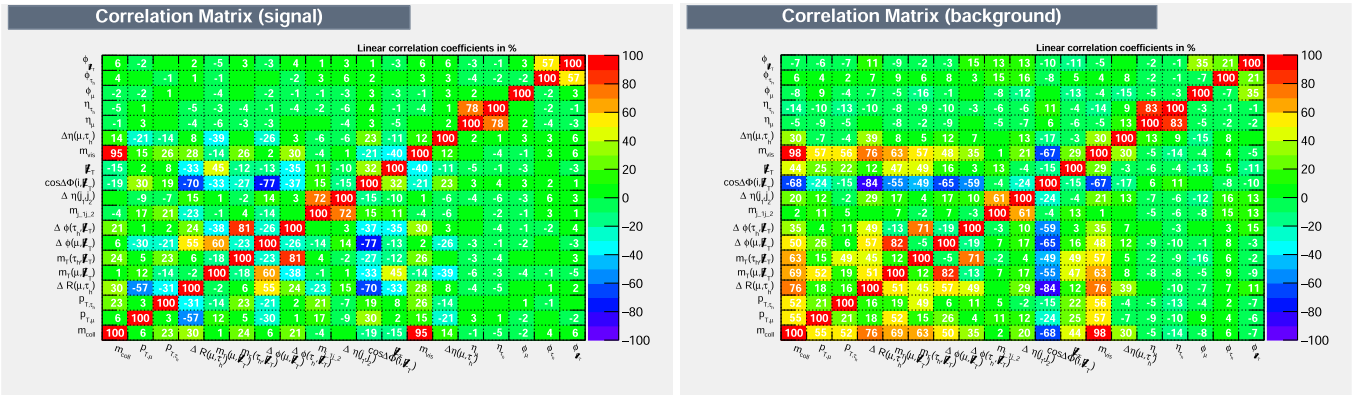

FIG. 4. Linear correlation coefficient matrix for input variables to the BDT for signal and background events in the $\mu\tau_h$ channel.

$W+$ jets background relevant for the $\mu\tau_h$ channel is very challenging, and is mostly estimated through data-driven techniques which is beyond the scope of the present work. The simulated background used in our BDT analysis constitutes roughly 75% of the full background. Accordingly, the ratio of the left-out misidentified background and the simulated background contribution to the total background is around $1/3$. In order to account for the underestimated background rate, we adopt a simplistic approach of compounding the total yield from other simulated background processes after the optimized BDT analysis by a factor of $(1+1/3)=4/3$. It must be noted that the inclusion of misidentified events in the BDT optimization itself might lead to marginally different sensitivity. As such, our results for the $\mu\tau_h$ channel are only conservative projections, and must be viewed as such.

The signal efficiency (ε_S) and background yields (B) at the HL-LHC from the BDT analysis are shown in Table III. Assuming SM rates for ggF and VBF Higgs production at $\sqrt{s}=14$ TeV, $\sigma^{\rm ggF}_{h_{\rm SM}}=49.5$ pb [computed at next-to-next-to-leading-order (NNLO) QCD + next-to-next-to-leading-logarithm QCD + next-to-leading-order (NLO) electroweak (EW)] and $\sigma^{\rm VBF}_{h_{\rm SM}}=4.2$ pb (computed at NNLO QCD + NLO EW) [93], the relative contribution from the ggF signal to the total signal rate is roughly 30% and 27% in the $\mu\tau_e$ and $\mu\tau_h$ channels, respectively. We translate the results into projected upper limits on the branching ratio for LFV Higgs decays in Table III using

$$\mathrm{Br}(h\to\mu\tau)=\frac{n_S\cdot\sqrt{B+(\kappa\cdot B)^2}}{\mathcal{L}\times(\sigma^{\rm ggF}_{h_{\rm SM}}\cdot\varepsilon^{\rm ggF}_S+\sigma^{\rm VBF}_{h_{\rm SM}}\cdot\varepsilon^{\rm VBF}_S)},\qquad(14)$$

where n_S is the standard deviation from background, and κ is the systematic uncertainty. We observe that the HL-LHC would be able to probe Higgs LFV decays in the VBF Higgs production channel up to $\mathrm{Br}(h\to\mu\tau)\sim 0.032\%$ at 2σ in a quasi-ideal scenario with no systematic uncertainties. The limit weakens to $\mathrm{Br}(h\to\mu\tau)\sim 0.1\%$ upon considering 5% systematic uncertainty. The current CMS limit on $\mathrm{Br}(h\to\mu\tau)$ from combined searches in $\mu\tau_e$, $\mu\tau_h$, $e\tau_\mu$ and $e\tau_h$ channels with ggF and VBF Higgs production, using the LHC run-II data collected at $\mathcal{L}=137$ fb^{-1}, is $\mathrm{Br}(h\to\mu\tau)<0.15\%$ at 95% C.L. [26]. The corresponding ATLAS limit is slightly weaker at $\mathrm{Br}(h\to\mu\tau)<0.18\%$ [94]. The projected reach at the HL-LHC from combined searches in the aforesaid channels with both ggF and VBF Higgs production has been estimated at $\mathrm{Br}(h\to\mu\tau)\lesssim 0.05\%$ in Ref. [95] through a luminosity scaling of the current limits, and is roughly 2 times stronger than the projected sensitivity derived in the present analysis for $\kappa=5\%$. Note that the search potential for the VBF channel alone is complementary to the combined projected reach.

TABLE III. Signal efficiency and background yields from searches for LFV decays of Higgs boson $pp\to(h\to\mu\tau)jj$ in the $\mu\tau_e$ and $\mu\tau_h$ channels at the $\sqrt{s}=14$ TeV LHC with $\mathcal{L}=3$ ab^{-1}. Projected upper limits (U.L.) on the LFV branching ratios are also shown for null and 5% systematic uncertainty.

	Signal efficiency			$\mathrm{Br}(h\to\mu\tau)(2\sigma)$ U.L.	
Channel	VBF	ggF	Background	$\kappa=0$	$\kappa=5\%$
$\mu\tau_e$	1.13×10^{-2}	4.5×10^{-4}	3192	5.4×10^{-4}	1.6×10^{-3}
$\mu\tau_h$	9.2×10^{-3}	3.0×10^{-4}	403	2.5×10^{-4}	3.5×10^{-4}
$\mu\tau_e+\mu\tau_h$ combined				3.2×10^{-4}	1.0×10^{-3}

The LFV Higgs branching fraction is related to the off-diagonal Yukawa couplings,

$$|Y_{\mu\tau}|^2+|Y_{\tau\mu}|^2=\frac{8\pi}{m_h}\frac{\mathrm{Br}(h\to\mu\tau)}{1-\mathrm{Br}(h\to\mu\tau)}\Gamma_h,\qquad(15)$$

where $\Gamma_h=4.07$ MeV [93] is the decay width for the SM Higgs boson. Using Eq. (15), upper limits on the LFV Higgs branching ratio can be translated into limits for $Y_{\mu\tau}$ and $Y_{\tau\mu}$, $\sqrt{|Y_{\mu\tau}|^2+|Y_{\tau\mu}|^2}<5.1\times10^{-4}$. We present these projected upper limits in the plane of $|Y_{\mu\tau}|$ and $|Y_{\tau\mu}|$ in Fig. 5 as solid-black lines. The current LHC limit at 95% C.L., $\sqrt{Y^2_{\mu\tau}+Y^2_{\tau\mu}}<1.1\times10^{-3}$ [26,96], is also shown as the shaded-black region with the current exclusion region displayed in shaded black. Other low-energy constraints and future projections discussed in Sec. II are also shown for comparison. The black-dashed line is the naturalness bound given in Eq. (3). It is clear that the HL-LHC projected sensitivities surpass the future low-energy constraints from $\tau\to\mu\gamma$ and $\tau\to3\mu$ expected at Belle II [97].

We also find from Fig. 5 that the current $(g-2)_\mu$ anomaly cannot be accommodated by LFV couplings of the SM Higgs boson, as the preferred region (green/yellow-shaded for $1\sigma/2\sigma$) is already excluded by both $\tau\to\mu\gamma$ constraint, as well as by the 13 TeV LHC upper limit on $\mathrm{Br}(h\to\mu\tau)$. It should however be noted that the significance of this anomaly has recently diminished, because of recent lattice developments [58–60]. So it remains to be seen whether we need any BSM physics in the muon $g-2$ sector.

IV. BSM HIGGS LFV DECAY AT THE HL-LHC

In this section, we further extend the analysis strategy discussed in Sec. III to study the projected sensitivity for LFV decays of a generic BSM leptophilic Higgs bosons H produced in the VBF mode, $pp\to Hjj\to(H\to\mu\tau)jj$, at the HL-LHC. Because of its leptophilic nature, the contributions from ggF Higgs production to the signal are not taken into account. We perform the BDT analysis for five signal benchmarks with $m_H<m_{h_{\rm SM}}$, $m_H=20$, 40, 60, 80 and 100 GeV, and five benchmarks with $m_H>m_{h_{\rm SM}}$, $m_H=150$, 200, 400, 600 and 800 GeV. Analogous to

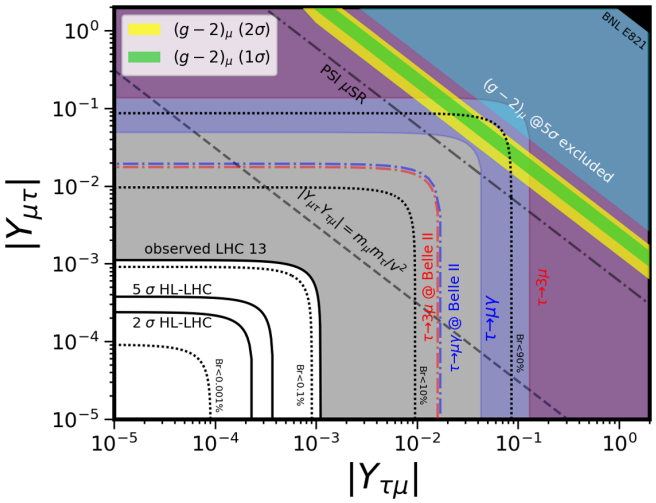

FIG. 5. Projected upper limits on the off-diagonal Yukawa couplings $|Y_{\mu\tau}|$ and $|Y_{\tau\mu}|$ from direct searches in the combined $\mu\tau_e + \mu\tau_h$ channel at the HL-LHC are represented as solid black lines (see also Table III). The current limit from 13 TeV LHC data [26] is shown by the black-shaded region. The red (blue) shaded region represents the exclusion from LFV decays $\tau \to 3\mu$ [75] ($\tau \to \mu\gamma$ [73]), whereas the red and blue dash-dotted lines are the corresponding future projected sensitivities at Belle II [98]. The green (yellow) band represents the preferred parameter space to accommodate the $(g-2)_\mu$ anomaly [53] at 1σ (2σ). The black and cyan shaded regions at the top right corner respectively represent the exclusions from μEDM [65] [only if $\Im(Y_{\mu\tau}Y_{\tau\mu}) \neq 0$] and $(g-2)_\mu$ [53] at 5σ, whereas the black dash-dotted diagonal line corresponds to the future sensitivity reach of μEDM [68] for $\Im(Y_{\mu\tau}Y_{\tau\mu})$. The black dashed diagonal line in the middle is the theoretical naturalness limit $Y_{\tau\mu}Y_{\mu\tau} = m_\mu m_\tau/v^2$ [18]. The dotted contours correspond to different values of the $h \to \mu\tau$ branching ratios (0.001%, 0.1%, 10% and 90%).

the earlier analysis, the search is performed in both $\mu\tau_h$ and $\mu\tau_e$ channels using the kinematic observables iterated in Table II. The observables found useful for our BDT analysis are identified in Tables IV and V for the $\mu\tau_e$ and $\mu\tau_h$ channels, respectively.

The signal efficiency and background yields at the HL-LHC from the BDT analysis in the $\mu\tau_h$ and $\mu\tau_e$ channels for various signal benchmarks are presented in Table VI. We translate the results into projected upper limits on the VBF Higgs production cross section times the branching ratio for LFV Higgs decays, $\sigma^{\rm VBF}_{H\to\mu\tau} = n_S\sqrt{B + (\kappa\cdot B)^2}/(\mathcal{L}\times\varepsilon_S^{\rm VBF})$, as a function of m_H. Projected upper limits at 2σ from searches in the $\mu\tau_e$ and $\mu\tau_h$ channels are shown in Table VI. Limits from combined searches in $\mu\tau_e + \mu\tau_h$ channels are also shown for $\kappa = 0$ and 5%. We observe that the projected limits get stronger with m_H except around $m_H \sim m_Z$ and $m_H \sim m_{h_{\rm SM}}$. For $m_H \sim m_Z$, the signal has a greater overlap with the $(Z \to \tau\tau) +$ jets background than the nearby signal benchmark points, which leads to a relatively lower signal efficiency. A similar albeit smaller decline in sensitivity occurs when the mass of the BSM Higgs boson is closer to $m_{h_{\rm SM}}$ due to greater overlap between the signal and the ggF/VBF $h \to \tau\tau$ backgrounds in the input dataset used for the BDT analysis, despite their subdominant contributions to the final event rate.

The combined search limits are interpolated to derive projected upper bounds on $\sigma^{\rm VBF}_{H\to\mu\tau}$ for $m_H \in [20, 800]$ GeV in Fig. 6 (left). It must be noted that the aforesaid projections are independent of any model considerations and can be translated to any new physics scenario in order

TABLE IV. Kinematic observables used in the BDT analysis for the $\mu\tau_e$ channel with different BSM Higgs boson masses. The used observables are marked with a ✓ (shows the six observables with the highest rank) or a •.

	m_H [GeV]										
$\mu\tau_e$	20	40	60	80	100	125	150	200	400	600	800
$p_{T,e}$	✓	•	•	•	•	•	•	•	•	•	
$m_T(e, \not{E}_T)$	✓	✓	•	✓	•	✓	✓	✓	✓	✓	✓
$\Delta R(\mu, e)$	✓	✓	✓	✓	✓	✓	✓	✓	•	•	•
$\Delta\phi(e, \not{E}_T)$		✓	•	•	✓	•	✓	•	•	✓	✓
$p_{T,\mu}$	•	•	✓	•	•	•	•	✓	✓	✓	✓
$m_T(\mu, \not{E}_T)$		•	•	•	•	✓	•	•	✓	✓	✓
$\Delta\phi(\mu, \not{E}_T)$			✓	✓	✓	✓	✓	✓	✓	✓	•
$m_{\rm coll}$		✓	✓	✓	✓	✓	✓	✓	✓	✓	✓
$m_{j_2 j_2}$	•	•	•	•	•	•	•	•	•	•	•
$\Delta\eta(j_1, j_2)$	✓	✓	✓	✓	✓	•	•	✓	✓	•	•
$\not{E}_T$	✓	✓	✓	✓	✓	✓	✓	•	•	•	✓
$p_{T,e}/p_{T,\mu}$	✓	•	•	•	•						

TABLE V. Kinematic observables used in the BDT analysis for the $\mu\tau_h$ channel with different BSM Higgs boson masses. The used observables are marked with a ✓ (shows the six observables with the highest rank) or a •.

	m_H [GeV]										
$\mu\tau_h$	20	40	60	80	100	125	150	200	400	600	800
p_{T,τ_h}	•	•	•	•	•	•	•	•	•	✓	✓
$m_T(\tau_h, \not{E}_T)$	•	•	•	•	•	✓	✓	✓	✓	✓	✓
$\Delta R(\mu, \tau_h)$		✓	•	•	•	•	•	•	•	•	•
η_{τ_h}		•	•	•	•	•	•	•	•	•	•
ϕ_{τ_h}	✓	•	•	✓	✓	•	•	•	•	•	•
$p_{T,\mu}$	•	•	•	•	•	•	•	•	✓	✓	✓
$m_T(\mu, \not{E}_T)$	•	•	•	•	•	•	•	✓	✓	✓	✓
$\Delta\phi(\mu, \not{E}_T)$	•	•	•	•	•	✓	✓	✓	✓	✓	✓
η_μ	✓	✓	✓	•	•	•	•	•	•	•	•
ϕ_μ	•	•	•	✓	✓	✓	✓	•	•	•	•
$\phi_{\not{E}_T}$	✓	•	✓	•	•	•	•	•	•	•	•
$m_{\rm coll}$	✓	✓	✓	✓	✓	✓	✓	✓	✓	✓	✓
$m_{j_1 j_2}$	•	•	•	•	•	•	•	•	•	•	•
$\Delta\eta(j_1, j_2)$	•	✓	✓	✓	✓	•	•	•	•	•	•
$\not{E}_T$	✓	✓	✓	✓	✓	✓	✓	✓	•	•	•
$\Delta\eta(\mu, \tau_h)$	✓	✓	✓	✓	✓	✓	✓	✓	✓	•	•

TABLE VI. Signal efficiency, background yields, and projected upper limits on $\sigma(pp \to Hjj) \times \mathrm{Br}(H \to \mu\tau)$ at 2σ, from searches for VBF Higgs production in the $\mu\tau_h$ and $\mu\tau_e$ channels at $\sqrt{s} = 14$ TeV LHC with $\mathcal{L} = 3$ ab^{-1}.

	$\mu\tau_h$			$\mu\tau_e$			$\mu\tau_e + \mu\tau_h$	
							2σ U.L. (fb)	
							κ	
m_H (GeV)	Signal efficiency (10^{-3})	Background	U.L. (2σ) (in fb)	Signal efficiency (10^{-3})	Background	U.L. (2σ) (in fb)	0	5%
20	0.46	11	4.8	6.7	557	2.3	1.6	2.1
40	4.4	26	0.77	5.4	250	1.9	0.55	0.60
60	5.3	81	1.1	3.8	641	4.4	0.90	1.1
80	2.1	32	1.8	5.6	1928	5.2	1.3	1.6
100	3.5	67	1.6	7.1	463	2.0	0.88	1.1
125	19.9	1603	1.3	9.4	1479	2.7	0.90	2.0
150	11.9	137	0.65	5.8	176	1.5	0.46	0.54
200	25.5	235	0.40	7.8	115	0.92	0.28	0.34
400	43.5	60	0.12	22.8	833	0.84	0.10	0.12
600	79.8	55	0.062	26.3	235	0.39	0.053	0.058
800	78.5	55	0.063	30.6	170	0.28	0.052	0.056

to test their projected reach at the HL-LHC. We observe that the HL-LHC would be able to probe LFV Higgs decays in VBF Higgs production up to $\sigma^{\mathrm{VBF}}_{H\to\mu\tau} \gtrsim 0.28(0.05)$ fb for $m_H = 200(800)$ GeV, at 2σ uncertainty. The projected sensitivity drops down to 0.34 and 0.056 upon considering 5% systematic uncertainty. Note that these projected limits are roughly 2 orders of magnitude smaller than the existing LHC limits on $\sigma(gg \to H) \times \mathrm{Br}(H \to \mu\tau)$ [35].

Considering SM-like VBF Higgs production rates, the above projections for $\kappa = 0$ are translated into upper limits on $\mathrm{Br}(H \to \mu\tau)$ in Fig. 6 (right). The projected sensitivity for $\mathrm{Br}(H \to \mu\tau)$ at the HL-LHC is roughly ∼0.0015% at $m_H = 300$ GeV, which weakens to ∼0.0030% as m_H increases to 800 GeV. At this point, we would like to note that the inclusion of ggF contributions to the VBF signal could further enhance the projected sensitivity, with the overall improvement being largely governed by the ratio of $\sigma^{\mathrm{ggF}}_H/\sigma^{\mathrm{VBF}}_H$.

To illustrate these constraints in a concrete model framework, we reinterpret them in a generic 2HDM [19,20] scenario, where the coupling of the SM-like Higgs boson h and the BSM Higgs boson H to weak bosons is $\sin(\beta-\alpha)$ and $\cos(\beta-\alpha)$ times the SM coupling, respectively, where β is the ratio of vacuum expectation values for the two Higgs doublets and α is the neutral Higgs mixing angle. Accordingly, in the 2HDM scenario, the VBF BSM Higgs production cross section can be parametrized as $\cos^2(\beta-\alpha)$ times the SM production rate. Using this analogy, we recast the upper limits on the VBF production cross section $\sigma(pp \to Hjj)$ times the branching ratio $\mathrm{Br}(H \to \mu\tau)$ into projections in the plane of $|\sin(\beta-\alpha)|$ and $\mathrm{Br}(H \to \mu\tau)$ for several BSM Higgs masses, as shown

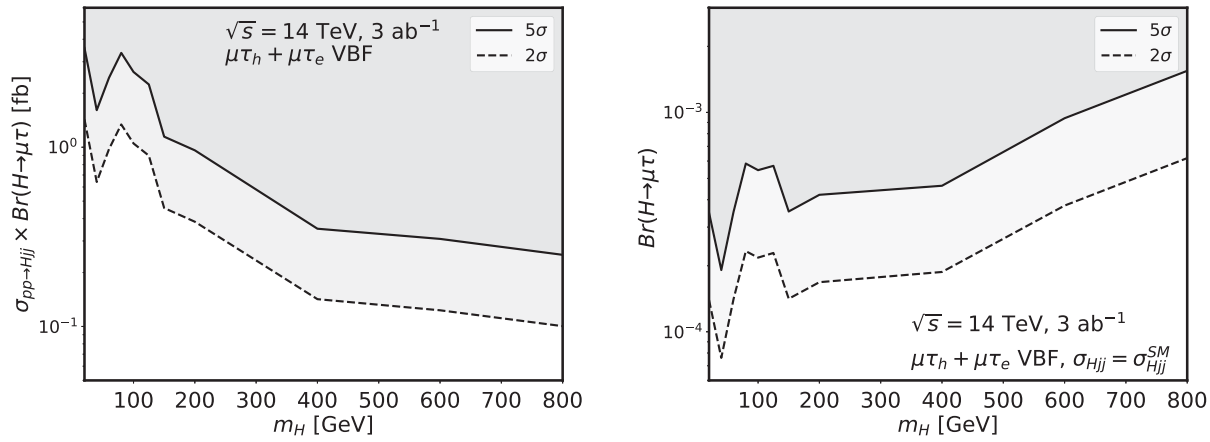

FIG. 6. Left: projected upper limits on the production cross section for the Higgs boson in the vector boson fusion mode times the branching ratio for LFV decays of the BSM Higgs boson, $\sigma^{\mathrm{VBF}}_{H\to\mu\tau}$, from combined searches in the $\mu\tau_e + \mu\tau_h$ channels at the $\sqrt{s} =$ 14 TeV at $\mathcal{L} = 3$ ab^{-1}. Right: projected upper limits on the left panel are translated into upper bounds on $\mathrm{Br}(H \to \mu\tau)$ considering SM-like vector boson fusion Higgs production rates.

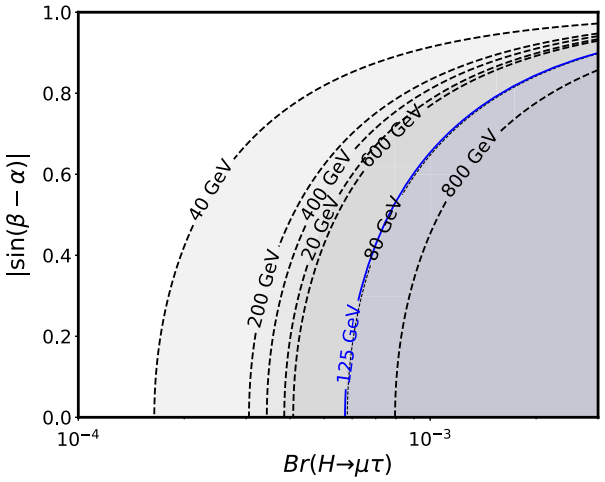

FIG. 7. Projected reach at 5σ in the plane of $|\sin(\beta-\alpha)|$ and $\mathrm{Br}(H\to\mu\tau)$ for a generic 2HDM scenario for different BSM Higgs masses from combined searches in the $\mu\tau_e+\mu\tau_h$ channels with VBF Higgs production at the $\sqrt{s}=14$ TeV at $\mathcal{L}=3$ ab^{-1}. The limit vanishes for $\sin(\beta-\alpha)\to 1$ [or $\cos(\beta-\alpha)\to 0$, the so-called alignment limit], in which case, the HWW coupling vanishes and there is no VBF production of H.

in Fig. 7. The shaded areas represent the projected exclusion regions at 5σ uncertainty for the respective values of m_H. It is important to note that the results in Fig. 7 are directly correlated to the projections for $\mathrm{Br}(H\to\mu\tau)$ shown in Fig. 6 (right). We observe that among the different representative signal benchmarks considered in the present analysis, the strongest sensitivity for $\mathrm{Br}(H\to\mu\tau)$ and henceforth, in the $\{|\sin(\beta-\alpha),\mathrm{Br}(H\to\mu\tau)|\}$ plane for a generic 2HDM model is observed for $m_H=40$ GeV. The sensitivity weakens as m_H approaches m_Z or m_h (as shown by the blue curve) due to a larger overlap with the backgrounds. Interestingly, the area of the projected exclusion region in the plane of $\{|\sin(\beta-\alpha),\mathrm{Br}(H\to\mu\tau)|\}$ improves with increasing m_H until around $m_H=150$ GeV beyond which the sensitivity again recedes gradually due to smaller cross sections.

The above result can be easily reinterpreted in different avatars of the 2HDM with LFV Higgs bosons [5,20,46,47,99–110]. For illustration, we consider two representative benchmarks, BP_I with $\cos(\beta-\alpha)=0.1$, $\tan\beta=6$, $m_H=400$ GeV in the type-I 2HDM, and BP_{II} with $\cos(\beta-\alpha)=0.05$, $\tan\beta=2.4$, $m_H=400$ GeV in the type-II 2HDM scenario, respectively. Both benchmarks are chosen from the parameter space allowed by the current Higgs global fit constraints [111]. We study the projected sensitivity for BP_I and BP_{II} from searches in the $\mu\tau_e+\mu\tau_h$ channels with VBF heavy Higgs production at the HL-LHC, using the results from our collider analysis (see Fig. 6). The projected sensitivities at the HL-LHC are presented in the plane of $|Y_{\mu\tau}|$ and $|Y_{\tau\mu}|$ in Fig. 8 as the solid-black curves. These are analogous to but weaker than the numbers shown in Fig. 5 for the 125 GeV Higgs case, mainly because the VBF production cross section for the Heavy Higgs boson is suppressed by a $\cos^2(\beta-\alpha)$ factor, as compared to the SM-like case.

In Fig. 8, the parameter space constrained by LFV decays $\tau\to 3\mu$ [75] and $\tau\to\mu\gamma$ [73] is shaded in red and blue, respectively, while their future reach at BELLE-II [98] is shown by the dashed curves. The green (yellow)-shaded area represents the parameter region consistent with the $(g-2)_\mu$ anomaly at $1(2)\sigma$. Here again, we observe that the

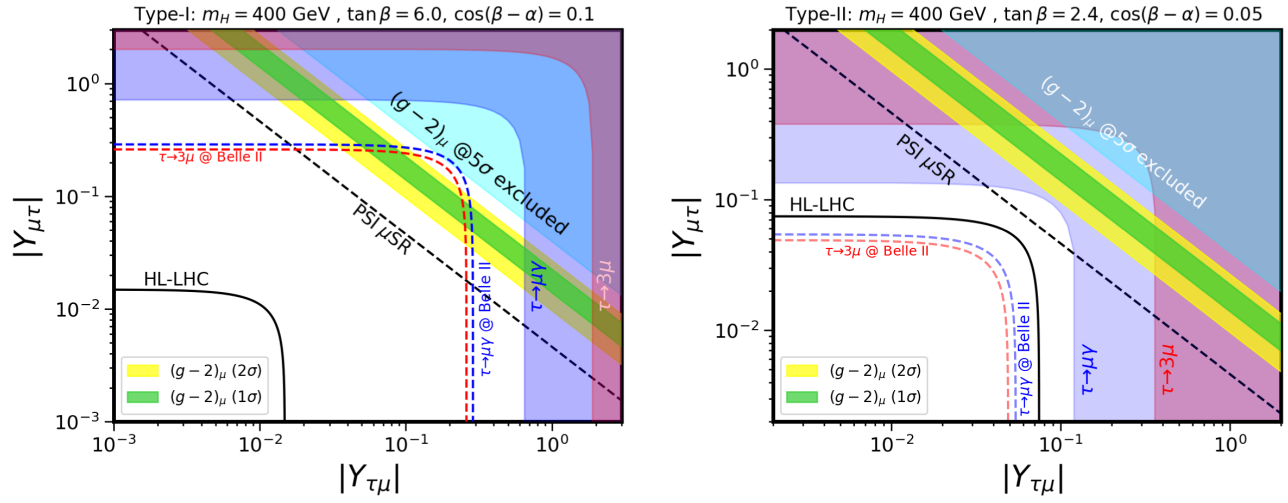

FIG. 8. Projected upper limits on the off-diagonal Yukawa couplings $|Y_{\mu\tau}|$ and $|Y_{\tau\mu}|$ from direct searches in the combined $\mu\tau_e+\mu\tau_h$ channel at the HL-LHC are represented as solid black lines. The red (blue) shaded region represents the exclusion from LFV decays $\tau\to 3\mu$ [75] ($\tau\to\mu\gamma$ [73]), whereas the red and blue dashed lines are the corresponding future projected sensitivities at Belle II [98]. The green (yellow) band represents the preferred parameter space to accommodate the $(g-2)_\mu$ anomaly [53] at 1σ (2σ). The black dashed line represents the future sensitivity reach of μEDM [68] for $\Im(Y_{\mu\tau}Y_{\tau\mu})$.

projected sensitivities at the HL-LHC exceed the future LFV reach of BELLE-II measurements for BP_I and they are comparable for BP_{II}. It is also worth noting that, unlike in the SM Higgs scenario, LFV can be further suppressed here by an appropriate choice of α and β, whereas the HL-LHC sensitivity is primarily determined by the combination $\beta - \alpha$. Moreover, for BP_I, we find that there is currently some allowed parameter space to explain the $(g-2)_\mu$ anomaly, which can be completely probed by HL-LHC.

Besides the 2HDM model, there are several other well-motivated extended Higgs sector models where LFV decays might naturally arise, such as in the little Higgs models [112–115], left-right symmetric models [116–120], mirror models [121–125], supersymmetric models [6,126–135], models with flavor symmetries [136], composite Higgs models [16,137], warped extra-dimension models [138–142], models with higher-dimensional operators [6,14,15,143,144], neutrino mass models [145–162] and other models [163–168]. The analysis presented in this section can be extended to these scenarios as well.

V. CONCLUSION

In this paper, we have examined the parameter space for LFV couplings of a neutral Higgs boson to muon and tau leptons. We show that these flavor violating couplings can be effectively probed at the HL-LHC through the VBF production process: $pp \to hjj \to (h \to \mu\tau)jj$, complementary to the ggF process. For the SM Higgs, we find $\sqrt{|Y_{\mu\tau}|^2 + |Y_{\tau\mu}|^2} < 5.1 \times 10^{-4}$ as the projected limit on the LFV Higgs Yukawa couplings, which turns out to be stronger than the existing and future limits from low-energy LFV observables like $\tau \to \mu\gamma$ and $\tau \to 3\mu$ (see Fig. 5). In addition, we have also studied the LFV arising from a generic BSM neutral Higgs boson H in the mass range of $m_H \in [20, 800]$ GeV and have given the projected model-independent upper limits on the VBF production cross section of Hjj times the branching ratio of $H \to \mu\tau$ at the HL-LHC (see Fig. 6). Finally, we have reinterpreted our results for the BSM neutral CP-even Higgs boson in the 2HDM (see Figs. 7 and 8). We find that HL-LHC will provide comparable or better constraints than the low-energy LFV searches on the LFV couplings of the BSM Higgs boson.

ACKNOWLEDGMENTS

R. K. B. thanks Biplob Bhattacherjee and Terrance Figy for helpful discussions. The work of R. K. B. is supported by the U.S. Department of Energy under Grant No. DE-SC0016013. Some of the computing for this project was performed at the High Performance Computing Center at Oklahoma State University, supported in part through the National Science Foundation Grant No. OAC-1531128. The work of B. D. was supported in part by the U.S. Department of Energy under Grant No. DE-SC0017987 and by a Universities Research Association Visiting Scholars Program Fellowship. B. D. acknowledges the Fermilab theory group for local hospitality during the completion of this work. A. T. acknowledges the Aspen Center of Physics for local hospitality during the completion of this work. The work at the Aspen Center for Physics is supported by National Science Foundation Grant No. PHY-1607611.

[1] G. Aad *et al.* (ATLAS Collaboration), Observation of a new particle in the search for the Standard Model Higgs boson with the ATLAS detector at the LHC, Phys. Lett. B **716**, 1 (2012).
[2] S. Chatrchyan *et al.* (CMS Collaboration), Observation of a new boson at a mass of 125 GeV with the CMS experiment at the LHC, Phys. Lett. B **716**, 30 (2012).
[3] ATLAS Collaboration, A detailed map of Higgs boson interactions by the ATLAS experiment ten years after the discovery, Nature (London) **607**, 52 (2022).
[4] CMS Collaboration, A portrait of the Higgs boson by the CMS experiment ten years after the discovery, Nature (London) **607**, 60 (2022).
[5] J. D. Bjorken and S. Weinberg, A Mechanism for Nonconservation of Muon Number, Phys. Rev. Lett. **38**, 622 (1977).
[6] J. L. Diaz-Cruz and J. J. Toscano, Lepton flavor violating decays of Higgs bosons beyond the Standard Model, Phys. Rev. D **62**, 116005 (2000).
[7] M. Raidal *et al.*, Flavour physics of leptons and dipole moments, Eur. Phys. J. C **57**, 13 (2008).
[8] G. Blankenburg, J. Ellis, and G. Isidori, Flavour-changing decays of a 125 GeV Higgs-like particle, Phys. Lett. B **712**, 386 (2012).
[9] R. Harnik, J. Kopp, and J. Zupan, Flavor violating Higgs decays, J. High Energy Phys. 03 (2013) 026.
[10] A. de Gouvea and P. Vogel, Lepton flavor and number conservation, and physics beyond the Standard Model, Prog. Part. Nucl. Phys. **71**, 75 (2013).
[11] A. Vicente, Lepton flavor violation beyond the MSSM, Adv. High Energy Phys. **2015**, 686572 (2015).
[12] M. Lindner, M. Platscher, and F. S. Queiroz, A call for new physics: The muon anomalous magnetic moment and lepton flavor violation, Phys. Rep. **731**, 1 (2018).
[13] W. Buchmuller and D. Wyler, Effective Lagrangian analysis of new interactions and flavor conservation, Nucl. Phys. **B268**, 621 (1986).

[14] K. S. Babu and S. Nandi, Natural fermion mass hierarchy and new signals for the Higgs boson, Phys. Rev. D **62**, 033002 (2000).
[15] G. F. Giudice and O. Lebedev, Higgs-dependent Yukawa couplings, Phys. Lett. B **665**, 79 (2008).
[16] K. Agashe and R. Contino, Composite Higgs-mediated FCNC, Phys. Rev. D **80**, 075016 (2009).
[17] J. Herrero-Garcia, N. Rius, and A. Santamaria, Higgs lepton flavour violation: UV completions and connection to neutrino masses, J. High Energy Phys. 11 (2016) 084.
[18] T. P. Cheng and M. Sher, Mass matrix ansatz and flavor nonconservation in models with multiple Higgs doublets, Phys. Rev. D **35**, 3484 (1987).
[19] T. D. Lee, A theory of spontaneous T violation, Phys. Rev. D **8**, 1226 (1973).
[20] G. C. Branco, P. M. Ferreira, L. Lavoura, M. N. Rebelo, M. Sher, and J. P. Silva, Theory and phenomenology of two-Higgs-doublet models, Phys. Rep. **516**, 1 (2012).
[21] A. Crivellin, J. Heeck, and P. Stoffer, A Perturbed Lepton-Specific Two-Higgs-Doublet Model Facing Experimental Lints for Physics Beyond the Standard Model, Phys. Rev. Lett. **116**, 081801 (2016).
[22] V. Khachatryan *et al.* (CMS Collaboration), Search for lepton flavour violating decays of the Higgs boson to $e\tau$ and $e\mu$ in proton-proton collisions at $\sqrt{s} = 8$ TeV, Phys. Lett. B **763**, 472 (2016).
[23] G. Aad *et al.* (ATLAS Collaboration), Search for lepton-flavour-violating decays of the Higgs and Z bosons with the ATLAS detector, Eur. Phys. J. C **77**, 70 (2017).
[24] A. M. Sirunyan *et al.* (CMS Collaboration), Search for lepton flavour violating decays of the Higgs boson to $\mu\tau$ and $e\tau$ in proton-proton collisions at $\sqrt{s} = 13$ TeV, J. High Energy Phys. 06 (2018) 001.
[25] G. Aad *et al.* (ATLAS Collaboration), Searches for lepton-flavour-violating decays of the Higgs boson in $\sqrt{s} =$ 13 TeV pp collisions with the ATLAS detector, Phys. Lett. B **800**, 135069 (2020).
[26] A. M. Sirunyan *et al.* (CMS Collaboration), Search for lepton-flavor violating decays of the Higgs boson in the $\mu\tau$ and $e\tau$ final states in proton-proton collisions at $\sqrt{s} = 13$ TeV, Phys. Rev. D **104**, 032013 (2021).
[27] V. Khachatryan *et al.* (CMS Collaboration), Search for lepton-flavour-violating decays of the Higgs boson, Phys. Lett. B **749**, 337 (2015).
[28] G. Aad *et al.* (ATLAS Collaboration), Search for lepton-flavour-violating $H \to \mu\tau$ decays of the Higgs boson with the ATLAS detector, J. High Energy Phys. 11 (2015) 211.
[29] G. Aad *et al.* (ATLAS Collaboration), Search for a Heavy Neutral Particle Decaying to $e\mu$, $e\tau$, or $\mu\tau$ in pp Collisions at $\sqrt{s} = 8$ TeV with the ATLAS Detector, Phys. Rev. Lett. **115**, 031801 (2015).
[30] M. Aaboud *et al.* (ATLAS Collaboration), Search for new phenomena in different-flavour high-mass dilepton final states in pp collisions at $\sqrt{s} = 13$ TeV with the ATLAS detector, Eur. Phys. J. C **76**, 541 (2016).
[31] A. M. Sirunyan *et al.* (CMS Collaboration), Search for lepton-flavor violating decays of heavy resonances and quantum black holes to $e\mu$ final states in proton-proton collisions at $\sqrt{s} = 13$ TeV, J. High Energy Phys. 04 (2018) 073.
[32] M. Aaboud *et al.* (ATLAS Collaboration), Search for lepton-flavor violation in different-flavor, high-mass final states in pp collisions at $\sqrt{s} = 13$ TeV with the ATLAS detector, Phys. Rev. D **98**, 092008 (2018).
[33] CMS Collaboration, Search for heavy resonances and quantum black holes in $e\mu$, $e\tau$, and $\mu\tau$ final states in proton-proton collisions at $\sqrt{s} = 13$ TeV, arXiv:2205.06709.
[34] R. Aaij *et al.* (LHCb Collaboration), Search for lepton-flavour-violating decays of Higgs-like bosons, Eur. Phys. J. C **78**, 1008 (2018).
[35] A. M. Sirunyan *et al.* (CMS Collaboration), Search for lepton flavour violating decays of a neutral heavy Higgs boson to $\mu\tau$ and $e\tau$ in proton-proton collisions at $\sqrt{s} = 13$ TeV, J. High Energy Phys. 03 (2020) 103.
[36] I. Chakraborty, A. Datta, and A. Kundu, Lepton flavor violating Higgs boson decay $\boldsymbol{h} \to \mu\tau$ at the ILC, J. Phys. G **43**, 125001 (2016).
[37] P. S. B. Dev, R. N. Mohapatra, and Y. Zhang, Lepton Flavor Violation Induced by a Neutral Scalar at Future Lepton Colliders, Phys. Rev. Lett. **120**, 221804 (2018).
[38] I. Chakraborty, S. Mondal, and B. Mukhopadhyaya, Lepton flavor violating Higgs boson decay at e^+e^- colliders, Phys. Rev. D **96**, 115020 (2017).
[39] Q. Qin, Q. Li, C.-D. Lü, F.-S. Yu, and S.-H. Zhou, Charged lepton flavor violating Higgs decays at future e^+e^- colliders, Eur. Phys. J. C **78**, 835 (2018).
[40] T. Li and M. A. Schmidt, Sensitivity of future lepton colliders to the search for charged lepton flavor violation, Phys. Rev. D **99**, 055038 (2019).
[41] B. Bhattacherjee, S. Chakraborty, and S. Mukherjee, Lepton flavour violating decay of 125 GeV Higgs boson to $\mu\tau$ channel and excess in $t\bar{t}H$, Mod. Phys. Lett. A **31**, 1650174 (2016).
[42] S. Banerjee, B. Bhattacherjee, M. Mitra, and M. Spannowsky, The lepton flavour violating Higgs decays at the HL-LHC and the ILC, J. High Energy Phys. 07 (2016) 059.
[43] K. Huitu, V. Keus, N. Koivunen, and O. Lebedev, Higgs-flavon mixing and $h \to \mu\tau$, J. High Energy Phys. 05 (2016) 026.
[44] E. Arganda, X. Marcano, N. I. Mileo, R. A. Morales, and A. Szynkman, Model-independent search strategy for the lepton-flavor-violating heavy Higgs boson decay to $\tau\mu$ at the LHC, Eur. Phys. J. C **79**, 738 (2019).
[45] U. Chattopadhyay, D. Das, and S. Mukherjee, Probing lepton flavor violating decays in MSSM with non-holomorphic soft terms, J. High Energy Phys. 06 (2020) 015.
[46] N. Ghosh and J. Lahiri, Revisiting a generalized two-Higgs-doublet model in light of the muon anomaly and lepton flavor violating decays at the HL-LHC, Phys. Rev. D **103**, 055009 (2021).
[47] N. Ghosh and J. Lahiri, Generalized 2HDM with wrong-sign lepton-Yukawa coupling, in light of $g_\mu - 2$ and lepton flavor violation at the future LHC, Eur. Phys. J. C **81**, 1074 (2021).
[48] K. Asai, J. Fujimoto, K. Kaneta, Y. Kurihara, and S. Tsuno, Measuring lepton flavor violation at the LHC, Phys. Rev. D **106**, 075014 (2022).
[49] M. A. Arroyo-Ureña, T. A. Valencia-Pérez, R. Gaitán, J. H. Montes De Oca, and A. Fernández-Téllez, Flavor-changing

decay $h \to \tau\mu$ at super hadron colliders, J. High Energy Phys. 08 (2020) 170.
[50] W.-s. Hou, R. Jain, and C. Kao, Searching for extra Higgs bosons via $pp \to H, A \to \tau\mu, \tau\tau$ at the Large Hadron Collider, arXiv:2202.04336.
[51] S. Dittmaier *et al.* (LHC Higgs Cross Section Working Group), *Handbook of LHC Higgs Cross Sections: 1. Inclusive Observables* (CERN, Geneva, 2011).
[52] D. Das, Dominant production of heavier Higgs bosons through vector boson fusion in the NMSSM, Phys. Rev. D **99**, 095035 (2019).
[53] B. Abi *et al.* (Muon $g-2$ Collaboration), Measurement of the Positive Muon Anomalous Magnetic Moment to 0.46 ppm, Phys. Rev. Lett. **126**, 141801 (2021).
[54] V. Andreev *et al.* (ACME Collaboration), Improved limit on the electric dipole moment of the electron, Nature (London) **562**, 355 (2018).
[55] J. P. Leveille, The second order weak correction to (G-2) of the muon in arbitrary gauge models, Nucl. Phys. **B137**, 63 (1978).
[56] G. W. Bennett *et al.* (Muon $g-2$ Collaboration), Final report of the muon E821 anomalous magnetic moment measurement at BNL, Phys. Rev. D **73**, 072003 (2006).
[57] T. Aoyama *et al.*, The anomalous magnetic moment of the muon in the Standard Model, Phys. Rep. **887**, 1 (2020).
[58] S. Borsanyi *et al.*, Leading hadronic contribution to the muon magnetic moment from lattice QCD, Nature (London) **593**, 51 (2021).
[59] M. Cè *et al.*, Window observable for the hadronic vacuum polarization contribution to the muon $g-2$ from lattice QCD, Phys. Rev. D **106**, 114502 (2022).
[60] C. Alexandrou *et al.*, Lattice calculation of the short and intermediate time-distance hadronic vacuum polarization contributions to the muon magnetic moment using twisted-mass fermions, arXiv:2206.15084.
[61] A. Crivellin, M. Hoferichter, C. A. Manzari, and M. Montull, Hadronic Vacuum Polarization: $(g-2)_\mu$ versus Global Electroweak Fits, Phys. Rev. Lett. **125**, 091801 (2020).
[62] A. Keshavarzi, W. J. Marciano, M. Passera, and A. Sirlin, Muon $g-2$ and $\Delta\alpha$ connection, Phys. Rev. D **102**, 033002 (2020).
[63] G. Colangelo, M. Hoferichter, and P. Stoffer, Constraints on the two-pion contribution to hadronic vacuum polarization, Phys. Lett. B **814**, 136073 (2021).
[64] G. Ecker, W. Grimus, and H. Neufeld, The neutron electric dipole moment in left-right symmetric gauge models, Nucl. Phys. **B229**, 421 (1983).
[65] G. W. Bennett *et al.* (Muon $g-2$ Collaboration), An improved limit on the muon electric dipole moment, Phys. Rev. D **80**, 052008 (2009).
[66] M. Abe *et al.*, A new approach for measuring the muon anomalous magnetic moment and electric dipole moment, Prog. Theor. Exp. Phys. **2019**, 053C02 (2019).
[67] Y. Sato (J-PARC E34 Collaboration), J-PARC Muon $g-2$/EDM experiment, J. Phys. Soc. Jpn. Conf. Proc. **33**, 011110 (2021).
[68] A. Adelmann *et al.*, Search for a muon EDM using the frozen-spin technique, arXiv:2102.08838.
[69] H. Albrecht *et al.* (ARGUS Collaboration), A search for the electric dipole moment of the tau lepton, Phys. Lett. B **485**, 37 (2000).
[70] K. Inami *et al.* (Belle Collaboration), Search for the electric dipole moment of the τ lepton, Phys. Lett. B **551**, 16 (2003).
[71] W. Bernreuther, L. Chen, and O. Nachtmann, Electric dipole moment of the tau lepton revisited, Phys. Rev. D **103**, 096011 (2021).
[72] L. Lavoura, General formulae for $f(1) \to f(2)$ gamma, Eur. Phys. J. C **29**, 191 (2003).
[73] B. Aubert *et al.* (*BABAR* Collaboration), Searches for Lepton Flavor Violation in the Decays $\tau^\pm \to e^\pm\gamma$ and $\tau^\pm \to \mu^\pm\gamma$, Phys. Rev. Lett. **104**, 021802 (2010).
[74] Y. Cai, J. Herrero-García, M. A. Schmidt, A. Vicente, and R. R. Volkas, From the trees to the forest: A review of radiative neutrino mass models, Front. Phys. **5**, 63 (2017).
[75] K. Hayasaka *et al.*, Search for lepton flavor violating τdecays into three leptons with 719 million produced $\tau^+\tau^-$ pairs, Phys. Lett. B **687**, 139 (2010).
[76] T. Goto, R. Kitano, and S. Mori, Lepton flavor violating Z-boson couplings from nonstandard Higgs interactions, Phys. Rev. D **92**, 075021 (2015).
[77] M. Dam, Tau-lepton physics at the FCC-ee circular e^+e^- collider, SciPost Phys. Proc. **1**, 041 (2019).
[78] G. Aad *et al.* (ATLAS Collaboration), Search for charged-lepton-flavour violation in Z-boson decays with the ATLAS detector, Nat. Phys. **17**, 819 (2021).
[79] A. Abada *et al.* (FCC Collaboration), FCC-ee: The lepton collider: Future circular collider conceptual design report Volume 2, Eur. Phys. J. Special Topics **228**, 261 (2019).
[80] I. Zurbano Fernandez *et al.*, High-Luminosity Large Hadron Collider (HL-LHC): Technical design report, CERN-2020-010, 2020.
[81] V. Del Duca, W. Kilgore, C. Oleari, C. Schmidt, and D. Zeppenfeld, Higgs + 2 Jets via Gluon Fusion, Phys. Rev. Lett. **87**, 122001 (2001).
[82] R. K. Barman, C. Englert, D. Gonçalves, and M. Spannowsky, Di-Higgs resonance searches in weak boson fusion, Phys. Rev. D **102**, 055014 (2020).
[83] J. Alwall, R. Frederix, S. Frixione, V. Hirschi, F. Maltoni, O. Mattelaer, H. S. Shao, T. Stelzer, P. Torrielli, and M. Zaro, The automated computation of tree-level and next-to-leading order differential cross sections, and their matching to parton shower simulations, J. High Energy Phys. 07 (2014) 079.
[84] P. Artoisenet, R. Frederix, O. Mattelaer, and R. Rietkerk, Automatic spin-entangled decays of heavy resonances in Monte Carlo simulations, J. High Energy Phys. 03 (2013) 015.
[85] J. Alwall *et al.*, Comparative study of various algorithms for the merging of parton showers and matrix elements in hadronic collisions, Eur. Phys. J. C **53**, 473 (2008).
[86] T. Sjostrand, S. Mrenna, and P. Z. Skands, A brief introduction to PYTHIA 8.1, Comput. Phys. Commun. **178**, 852 (2008).
[87] J. de Favereau, C. Delaere, P. Demin, A. Giammanco, V. Lemaître, A. Mertens, and M. Selvaggi (DELPHES 3 Collaboration), DELPHES 3, A modular framework for fast

simulation of a generic collider experiment, J. High Energy Phys. 02 (2014) 057.
[88] M. Cepeda *et al.*, Report from working group 2: Higgs physics at the HL-LHC and HE-LHC, CERN Yellow Rep. Monogr. **7**, 221 (2019).
[89] https://github.com/delphes/delphes/releases/tag/3.4.2pre16.
[90] R. Ellis, I. Hinchliffe, M. Soldate, and J. Van Der Bij, Higgs decay to $\tau^+\tau^-$: A possible signature of intermediate mass higgs bosons at high energy hadron colliders, Nucl. Phys. **B297**, 221 (1988).
[91] A. Elagin, P. Murat, A. Pranko, and A. Safonov, A new mass reconstruction technique for resonances Decaying to di-tau, Nucl. Instrum. Methods Phys. Res., Sect. A **654**, 481 (2011).
[92] K. Hagiwara, K. Ma, and S. Mori, Probing *CP* Violation in $h \to \tau^-\tau^+$ at the LHC, Phys. Rev. Lett. **118**, 171802 (2017).
[93] J. R. Andersen *et al.* (LHC Higgs Cross Section Working Group), Handbook of LHC Higgs cross sections: 3. Higgs properties, arXiv:1307.1347.
[94] ATLAS Collaboration, Searches for lepton-flavour-violating decays of the Higgs boson into $e\tau$ and $\mu\tau$ in $\sqrt{s} = 13$ TeV pp collisions with the ATLAS detector, Report No. ATLAS-CONF-2022-060.
[95] T. Davidek and L. Fiorini, Search for lepton-flavor-violating decays of bosons with the ATLAS detector, Front. Phys. **8**, 149 (2020).
[96] ATLAS Collaboration, Searches for lepton-flavour-violating decays of the Higgs boson into $e\tau$ and $\mu\tau$ in $\sqrt{s} = 13$ TeV pp collisions with the ATLAS detector, Technical Report, CERN, Geneva, 2022, http://cds.cern.ch/record/2826869.
[97] W. Altmannshofer *et al.* (Belle-II Collaboration), The Belle II physics book, Prog. Theor. Exp. Phys. **2019**, 123C01 (2019); **2020**, 029201(E) (2020).
[98] L. Aggarwal *et al.* (Belle-II Collaboration), Snowmass White Paper: Belle II physics reach and plans for the next decade and beyond, arXiv:2207.06307.
[99] S. Davidson and G. J. Grenier, Lepton flavour violating Higgs and tau to mu gamma, Phys. Rev. D **81**, 095016 (2010).
[100] J. Kopp and M. Nardecchia, Flavor and *CP* violation in Higgs decays, J. High Energy Phys. 10 (2014) 156.
[101] Y. Omura, E. Senaha, and K. Tobe, Lepton-flavor-violating Higgs decay $h \to \mu\tau$ and muon anomalous magnetic moment in a general two Higgs doublet model, J. High Energy Phys. 05 (2015) 028.
[102] F. J. Botella, G. C. Branco, M. Nebot, and M. N. Rebelo, Flavour changing Higgs couplings in a class of two Higgs doublet models, Eur. Phys. J. C **76**, 161 (2016).
[103] M. Buschmann, J. Kopp, J. Liu, and X.-P. Wang, New signatures of flavor violating Higgs couplings, J. High Energy Phys. 06 (2016) 149.
[104] W. Altmannshofer, J. Eby, S. Gori, M. Lotito, M. Martone, and D. Tuckler, Collider signatures of flavorful Higgs bosons, Phys. Rev. D **94**, 115032 (2016).
[105] R. Primulando and P. Uttayarat, Probing lepton flavor violation at the 13 TeV LHC, J. High Energy Phys. 05 (2017) 055.
[106] A. Crivellin, D. Müller, and C. Wiegand, $b \to s\ell^+\ell^-$ transitions in two-Higgs-doublet models, J. High Energy Phys. 06 (2019) 119.
[107] S. Iguro, Y. Omura, and M. Takeuchi, Testing the 2HDM explanation of the muon $g-2$ anomaly at the LHC, J. High Energy Phys. 11 (2019) 130.
[108] A. Vicente, Higgs lepton flavor violating decays in two Higgs doublet models, Front. Phys. **7**, 174 (2019).
[109] R. Primulando, J. Julio, and P. Uttayarat, Collider constraints on lepton flavor violation in the 2HDM, Phys. Rev. D **101**, 055021 (2020).
[110] M. Blanke and S. Iguro, Collider probe of heavy additional Higgs bosons solving the muon $g-2$, arXiv:2210.13508.
[111] F. Kling, S. Su, and W. Su, 2HDM neutral scalars under the LHC, J. High Energy Phys. 06 (2020) 163.
[112] B. Yang, J. Han, and N. Liu, Lepton flavor violating Higgs boson decay $h \to \mu\tau$ in the littlest Higgs model with T parity, Phys. Rev. D **95**, 035010 (2017).
[113] F. del Aguila, L. Ametller, J. I. Illana, J. Santiago, P. Talavera, and R. Vega-Morales, The full lepton flavor of the littlest Higgs model with T-parity, J. High Energy Phys. 07 (2019) 154.
[114] I. Pacheco and P. Roig, Lepton flavor violation in the littlest Higgs model with T parity realizing an inverse seesaw, J. High Energy Phys. 02 (2022) 054.
[115] E. Ramirez and P. Roig, Lepton flavor violation within the simplest little Higgs model, Phys. Rev. D **106**, 056018 (2022).
[116] P. S. B. Dev, R. N. Mohapatra, and Y. Zhang, Probing the Higgs sector of the minimal left-right symmetric model at future hadron colliders, J. High Energy Phys. 05 (2016) 174.
[117] A. Maiezza, G. Senjanović, and J. C. Vasquez, Higgs sector of the minimal left-right symmetric theory, Phys. Rev. D **95**, 095004 (2017).
[118] P. S. B. Dev, R. N. Mohapatra, and Y. Zhang, Displaced photon signal from a possible light scalar in minimal left-right seesaw model, Phys. Rev. D **95**, 115001 (2017).
[119] P. S. B. Dev, R. N. Mohapatra, and Y. Zhang, Long Lived Light Scalars as Probe of Low Scale Seesaw Models, Nucl. Phys. **B923**, 179 (2017).
[120] O. M. Boyarkin, G. G. Boyarkina, and D. S. Vasileuskaya, The Higgs boson decays with the lepton flavor violation, Int. J. Mod. Phys. A **33**, 1850103 (2018).
[121] P. Q. Hung, A Model of electroweak-scale right-handed neutrino mass, Phys. Lett. B **649**, 275 (2007).
[122] P. Q. Hung, Electroweak-scale mirror fermions, $\mu \to e\gamma$ and $\tau \to mu\gamma$, Phys. Lett. B **659**, 585 (2008).
[123] J.-P. Bu, Y. Liao, and J.-Y. Liu, Lepton flavor violating muon decays in a model of electroweak-scale right-handed neutrinos, Phys. Lett. B **665**, 39 (2008).
[124] C.-F. Chang, C.-H. V. Chang, C. S. Nugroho, and T.-C. Yuan, Lepton flavor violating decays of neutral Higgses in extended mirror Fermion model, Nucl. Phys. **B910**, 293 (2016).
[125] P. Q. Hung, T. Le, V. Q. Tran, and T.-C. Yuan, Muon-to-electron conversion in mirror fermion model with electroweak scale non-sterile right-handed neutrinos, Nucl. Phys. **B932**, 471 (2018).
[126] T. Han and D. Marfatia, $h \to \mu\tau$ at Hadron Colliders, Phys. Rev. Lett. **86**, 1442 (2001).
[127] J. L. Diaz-Cruz, D. K. Ghosh, and S. Moretti, Lepton flavour violating heavy Higgs decays within the νMSSM

and their detection at the LHC, Phys. Lett. B **679**, 376 (2009).
[128] A. Arhrib, Y. Cheng, and O. C. W. Kong, Comprehensive analysis on lepton flavor violating Higgs boson to $\mu^{\mp}\tau^{\pm}$ decay in supersymmetry without R parity, Phys. Rev. D **87**, 015025 (2013).
[129] M. Arana-Catania, E. Arganda, and M. J. Herrero, Non-decoupling SUSY in LFV Higgs decays: A window to new physics at the LHC, J. High Energy Phys. 09 (2013) 160; 10 (2015) 192(E).
[130] D. Aloni, Y. Nir, and E. Stamou, Large BR$(h \to \tau\mu)$ in the MSSM?, J. High Energy Phys. 04 (2016) 162.
[131] H.-B. Zhang, T.-F. Feng, S.-M. Zhao, Y.-L. Yan, and F. Sun, 125 GeV Higgs decay with lepton flavor violation in the $\mu\nu$SSM, Chin. Phys. C **41**, 043106 (2017).
[132] S. V. Demidov and I. V. Sobolev, Lepton flavor-violating decays of the Higgs boson from sgoldstino mixing, J. High Energy Phys. 08 (2016) 030.
[133] X.-X. Dong, S.-M. Zhao, H.-B. Zhang, and T.-F. Feng, Charged lepton flavor violation in extended BLMSSM, Eur. Phys. J. C **79**, 17 (2019).
[134] Z.-N. Zhang, H.-B. Zhang, J.-L. Yang, S.-M. Zhao, and T.-F. Feng, Higgs boson decays with lepton flavor violation in the $B-L$ symmetric SSM, Phys. Rev. D **103**, 115015 (2021).
[135] Y.-T. Wang, S.-M. Zhao, T.-T. Wang, X. Wang, X.-X. Long, J. Ma, and T.-F. Feng, Z boson decays $Z \to li \pm lj \mp$ and Higgs boson decays $h \to li \pm lj \mp$ with lepton flavor violation in a U(1) extension of the MSSM, Phys. Rev. D **106**, 055044 (2022).
[136] H. Ishimori, T. Kobayashi, H. Ohki, Y. Shimizu, H. Okada, and M. Tanimoto, Non-Abelian discrete symmetries in particle physics, Prog. Theor. Phys. Suppl. **183**, 1 (2010).
[137] A. Azatov, M. Toharia, and L. Zhu, Higgs mediated FCNC's in warped extra dimensions, Phys. Rev. D **80**, 035016 (2009).
[138] G. Perez and L. Randall, Natural neutrino masses and mixings from warped geometry, J. High Energy Phys. 01 (2009) 077.
[139] S. Casagrande, F. Goertz, U. Haisch, M. Neubert, and T. Pfoh, Flavor physics in the Randall-Sundrum model: I. Theoretical setup and electroweak precision tests, J. High Energy Phys. 10 (2008) 094.
[140] M. Blanke, A. J. Buras, B. Duling, S. Gori, and A. Weiler, $\Delta F = 2$ observables and fine-tuning in a warped extra dimension with custodial protection, J. High Energy Phys. 03 (2009) 001.
[141] M. E. Albrecht, M. Blanke, A. J. Buras, B. Duling, and K. Gemmler, Electroweak and flavour structure of a warped extra dimension with custodial protection, J. High Energy Phys. 09 (2009) 064.
[142] A. J. Buras, B. Duling, and S. Gori, The impact of Kaluza-Klein fermions on standard model fermion couplings in a RS model with custodial protection, J. High Energy Phys. 09 (2009) 076.
[143] J. A. Aguilar-Saavedra, A Minimal set of top-Higgs anomalous couplings, Nucl. Phys. **B821**, 215 (2009).
[144] A. Goudelis, O. Lebedev, and J.-h. Park, Higgs-induced lepton flavor violation, Phys. Lett. B **707**, 369 (2012).
[145] A. Pilaftsis, Lepton flavor nonconservation in H0 decays, Phys. Lett. B **285**, 68 (1992).
[146] J. G. Korner, A. Pilaftsis, and K. Schilcher, Leptonic CP asymmetries in flavor changing H0 decays, Phys. Rev. D **47**, 1080 (1993).
[147] E. Arganda, M. J. Herrero, X. Marcano, and C. Weiland, Imprints of massive inverse seesaw model neutrinos in lepton flavor violating Higgs boson decays, Phys. Rev. D **91**, 015001 (2015).
[148] E. Arganda, M. J. Herrero, X. Marcano, and C. Weiland, Enhancement of the lepton flavor violating Higgs boson decay rates from SUSY loops in the inverse seesaw model, Phys. Rev. D **93**, 055010 (2016).
[149] T. T. Thuc, L. T. Hue, H. N. Long, and T. P. Nguyen, Lepton flavor violating decay of SM-like Higgs boson in a radiative neutrino mass model, Phys. Rev. D **93**, 115026 (2016).
[150] M. Aoki, S. Kanemura, K. Sakurai, and H. Sugiyama, Testing neutrino mass generation mechanisms from the lepton flavor violating decay of the Higgs boson, Phys. Lett. B **763**, 352 (2016).
[151] E. Arganda, M. J. Herrero, X. Marcano, R. Morales, and A. Szynkman, Effective lepton flavor violating $H \ell i \ell j$ vertex from right-handed neutrinos within the mass insertion approximation, Phys. Rev. D **95**, 095029 (2017).
[152] J. Herrero-García, T. Ohlsson, S. Riad, and J. Wirén, Full parameter scan of the Zee model: Exploring Higgs lepton flavor violation, J. High Energy Phys. 04 (2017) 130.
[153] N. H. Thao, L. T. Hue, H. T. Hung, and N. T. Xuan, Lepton flavor violating Higgs boson decays in seesaw models: New discussions, Nucl. Phys. **B921**, 159 (2017).
[154] K. Enomoto, S. Kanemura, K. Sakurai, and H. Sugiyama, New model for radiatively generated Dirac neutrino masses and lepton flavor violating decays of the Higgs boson, Phys. Rev. D **100**, 015044 (2019).
[155] K. S. Babu, P. S. B. Dev, S. Jana, and A. Thapa, Non-standard interactions in radiative neutrino mass models, J. High Energy Phys. 03 (2020) 006.
[156] X. Marcano and R. A. Morales, Flavor techniques for LFV processes: Higgs decays in a general seesaw model, Front. Phys. **7**, 228 (2020).
[157] N. Haba, T. Omija, and T. Yamada, Charged lepton flavor violating processes in neutrinophilic Higgs + seesaw model, Prog. Theor. Exp. Phys. **2020**, 073B08 (2020).
[158] K. S. Babu, P. S. B. Dev, S. Jana, and A. Thapa, Unified framework for B-anomalies, muon $g-2$ and neutrino masses, J. High Energy Phys. 03 (2021) 179.
[159] R. K. Barman, R. Dcruz, and A. Thapa, Neutrino masses and magnetic moments of electron and muon in the Zee Model, J. High Energy Phys. 03 (2022) 183.
[160] R. S. Hundi, Lepton flavor violating Z and Higgs decays in the scotogenic model, Eur. Phys. J. C **82**, 505 (2022).
[161] J. Julio, S. Saad, and A. Thapa, Marriage between neutrino mass and flavor anomalies, Phys. Rev. D **106**, 055003 (2022).
[162] R. Dcruz and A. Thapa, W boson mass shift, dark matter and $(g-2)_{\ell}$ in ScotoZee model, Phys. Rev. D **107**, 015002 (2023).

[163] I. Doršner, S. Fajfer, A. Greljo, J. F. Kamenik, N. Košnik, and I. Nišandžic, New physics models facing lepton flavor violating Higgs decays at the percent level, J. High Energy Phys. 06 (2015) 108.

[164] S. Baek and Z.-F. Kang, Naturally large radiative lepton flavor violating Higgs decay mediated by lepton-flavored dark matter, J. High Energy Phys. 03 (2016) 106.

[165] L. T. Hue, H. N. Long, T. T. Thuc, and T. Phong Nguyen, Lepton flavor violating decays of Standard-Model-like Higgs in 3-3-1 model with neutral lepton, Nucl. Phys. **B907**, 37 (2016).

[166] C. Alvarado, R. M. Capdevilla, A. Delgado, and A. Martin, Minimal models of loop-induced lepton flavor violation in Higgs boson decays, Phys. Rev. D **94**, 075010 (2016).

[167] J. A. Evans, P. Tanedo, and M. Zakeri, Exotic lepton-flavor violating Higgs decays, J. High Energy Phys. 01 (2020) 028.

[168] T. T. Hong, H. T. Hung, H. H. Phuong, L. T. T. Phuong, and L. T. Hue, Lepton-flavor-violating decays of the SM-like Higgs boson $h \to e_i e_j$, and $e_i \to e_j \gamma$ in a flipped 3-3-1 model, Prog. Theor. Exp. Phys. **2020**, 043B03 (2020).